Development and initial assessment of [18F]OP-801: a novel hydroxyl dendrimer PET tracer for preclinical imaging of innate immune activation in the whole body and brain

Mackenzie L. Carlson
Stanford University School of Medicine
Isaac M. Jackson
Stanford University School of Medicine
E. Carmen Azevedo
Stanford University School of Medicine
Samantha T Reyes
Stanford University School of Medicine
Israt S Alam
Stanford University School of Medicine
Rowaid Kellow
Stanford University School of Medicine
Jessa B. Castillo
Stanford University School of Medicine
Sydney C Nagy
Stanford University School of Medicine
Rishi Sharma
Ashvattha Therapeutics
Matthew Brewer
Ashvattha Therapeutics
Jeffrey Cleland
Ashvattha Therapeutics
Bin Shen
Stanford University School of Medicine
Michelle James (mljames@stanford.edu)
Stanford University https://orcid.org/0000-0002-9934-7084

Research Article

Keywords: Neuroinflammation, PET, 18F, preclinical imaging, radiochemistry

Posted Date: August 1st, 2023

DOI: https://doi.org/10.21203/rs.3.rs-3186506/v1

Version of Record: A version of this preprint was published at Molecular Imaging and Biology on September 21st, 2023. See the published version at https://doi.org/10.1007/s11307-023-01850-5.

Abstract

Purpose

Innate immune activation plays a critical role in the onset and progression of many diseases. While positron emission tomography (PET) imaging provides a non-invasive means to visualize and quantify such immune responses, most available tracers are not specific for innate immune cells. To address this need, we developed [^{18}F]OP-801 by radiolabeling a novel hydroxyl dendrimer that is selectively taken up by reactive macrophages/microglia and evaluated its ability to detect innate immune activation in mice following lipopolysaccharide (LPS) challenge.

Procedures:

OP-801 was radiolabeled in two steps: [^{18}F]fluorination of a tosyl precursor to yield [^{18}F]3-fluoropropyl azide, followed by a copper-catalyzed click reaction. After purification and stability testing, [^{18}F]OP-801 (150–250 μCi) was intravenously injected into female C57BL/6 mice 24 hours after intraperitoneal administration of LPS (10 mg/kg, n = 14) or saline (n = 6). Upon completing dynamic PET/CT imaging, mice were perfused and radioactivity was measured in tissues of interest via gamma counting or autoradiography.

Results

[^{18}F]OP-801 was produced with > 95% radiochemical purity, 12–52 μCi/μg specific activity, and 4.3 ± 1.5% decay-corrected yield. *Ex vivo* metabolite analysis of plasma samples (n = 4) demonstrated high stability in mice (97 ± 3% intact tracer > 120 min post-injection). PET/CT images of mice following LPS challenge revealed higher signal in organs known to be inflamed in this context, including liver, lung, and spleen. Gamma counting confirmed PET findings, showing significantly elevated signal in the same tissues compared to saline-injected mice: liver (p = 0.009), lung (p = 0.030), and spleen (p = 0.004). Brain PET/CT images (summed 50–60 min) revealed linearly increasing [^{18}F]OP-801 uptake in whole brain that significantly correlated with murine sepsis score ($r = 0.85$, $p < 0.0001$). Specifically, tracer uptake was significantly higher in the brain stem, cortex, olfactory bulb, white matter, and ventricles of LPS-treated mice compared to saline-treated mice ($p < 0.05$).

Conclusion

[^{18}F]OP-801 is a promising new PET tracer for sensitive and specific detection of activated macrophages and microglia that warrants further investigation.

Introduction

Mounting evidence indicates that innate immune dysfunction, involving chronic activation of microglia (myeloid cells of the brain) and macrophages (myeloid cells that typically reside in peripheral tissues), plays a critical role in the onset and progression of many neurological diseases[1–3]. While positron emission tomography (PET) imaging provides a non-invasive method to visualize and quantify innate immune activation in the brain and periphery, most available PET tracers, such as those targeting translocator protein 18 kDa (TSPO), are not entirely specific for macrophages/microglia[4,5]. We identified OP-801, a new synthetic polyamidoamine (PAMAM) hydroxyl dendrimer that crosses the blood-brain barrier in the presence of inflammation and is selectively (> 95%) taken up by reactive macrophages/microglia[6], as a promising radiotracer candidate. We developed the first hydroxyl dendrimer PET tracer targeting reactive macrophages/microglia by radiolabeling OP-801 with fluorine-18 ($t_{1/2}$=109.8 min) and subsequently assessed its stability in mouse plasma, followed by evaluating its ability to detect inflammation in the brain and periphery of mice with lipopolysaccharide (LPS)-induced sepsis.

One key characteristic of an ideal neuroinflammatory PET tracer is the ability to detect maladaptive innate immune activation (activated microglia and macrophages), with high specificity and sensitivity to accurately inform scientists and clinicians on the spatiotemporal dynamics of toxic innate immune responses *in vivo*[7]. The current gold-standard PET targets for imaging neuroinflammation is TSPO, but this target suffers from significant drawbacks: of note, TSPO is expressed in multiple cell types (i.e., myeloid, endothelial, astrocytes, cancer) and has a poorly understood functional role in many disease processes of interest, including neurodegeneration[8]. Additionally, second generation TSPO tracers have low affinity binding for certain patients due to a genetic polymorphism, thus limiting their widespread implementation in clinical trials[9]. Other emerging neuroinflammatory biomarkers of interest (e.g. colony stimulating factor 1 receptor (CSF1R)[10], cannabinoid receptor type 2 (CB2R)[11], and P2X7) have relatively high baseline expression levels (in the CNS and/or periphery) and are not only expressed on microglia/macrophages, but also on astrocytes, neurons, and/or endothelial cells, meaning that PET tracers for these targets do not enable highly specific and sensitive detection of innate immune cells.

Our tracer, [^{18}F]OP-801, is a hydroxyl dendrimer made of repetitive branching units of methyl acrylate and ethylene diamine, with a molecular weight of ~ 15000 Da. Instead of targeting a specific gene or protein, OP-801 is able to cross the blood-brain barrier in the presence of neuroinflammation and is specifically taken up via fluid-phase endocytosis by activated macrophages/microglia throughout the body. The specificity of G4-OH PAMAM dendrimers for activated macrophages/microglia has been demonstrated through published mechanistic studies in over 30 animal models of neuroinflammation, including dogs and non-human primates[12–18]. In particular, the selectivity of OP-801 for activated macrophages/microglia has been shown by administering a Cy5 labelled version of OP-801 to the aforementioned animal models and conducting flow cytometric assays and fluorescent microscopy of inflamed brain tissue[6,19]. Importantly, there has been no observed uptake of such hydroxyl dendrimers occurring in normal cells, including oligodendrocytes, neurons, or peripheral resting macrophages[19]. We

hypothesize that [^{18}F]OP-801 can be used to non-invasively detect innate immune activation in a rodent model of LPS-induced sepsis in tissues known to be inflamed in this model (including the brain, lungs, and major abdominal organs). Additionally, we expect the amount of PET signal in the brain to correspond with the severity of sepsis-induced clinical symptoms, which can be measured using a standard murine sepsis scoring system.

Materials and Methods

Animals: Animal experiments were conducted in accordance with the Administrative Panel on Laboratory Animal Care (APLAC) at Stanford University), which is accredited by the Association for the Assessment and Accreditation of Laboratory Animal Care (AAALAC International). Female 4-4.5-month-old C57BL/6 wild-type mice (Jackson Laboratories) were housed in groups of 5, separated by disease category (LPS vs saline/control) in a temperature-controlled environment under a 12-hour light/dark schedule with ad libitum access to food and water. Female mice were selected since they typically are more resilient to LPS than males, and thus the immune response is slightly more subtle to detect and they are more able to withstand prolonged (> 1hr) aesthesia[20,21]. When indicated, anesthetization was performed using isoflurane (2-3.5% for induction, 1-2.5% for maintenance). There were no significant differences in weight between the groups of LPS and saline mice, as determined by student's T-test. The average weight of mice used in this study was 21.2 ± 0.89 g and 21.2 ± 1.93 g for saline and LPS groups respectively.

Radiochemistry: [^{18}F]OP-801 was radiolabeled in two steps: 1) Preparation of [^{18}F]3-Fluoropropylazide from 3-azidopropyl-4-methylbenzenesulfonate and no-carrier-added [^{18}F]fluoride in anhydrous acetonitrile and 2) copper-catalyzed click reaction (CuAAC) of alkyne functionalized hydroxyl dendrimer precursor (Ashvattha Therapeutics, Inc.) with [^{18}F]3-Fluoropropylazide in methanol (Scheme 1). [^{18}F]Fluoride was produced using a cyclotron (GE PETtrace) via the ^{18}O(p, n)^{18}F nuclear reaction, trapped on a ^{18}F separation cartridge (EMD), eluted with 1.0 mL of a solution containing K_2CO_3 (3.5 mg) and Kryptofix 2.2.2. (15 mg) in MeCN (0.90 mL) and water (0.10 mL). The mixture was heated and dried under vacuum/helium at 88 ^{o}C for 5 min, followed by cooling down the mixture to 60 ^{o}C. A solution of 3-azidopropyl-4-methylbenzenesulfonate (4 mg) in anhydrous dimethylsulfoxide (DMSO) (1 mL) was added to the dried ^{18}F/K222/K_2CO_3 complex and heated to 80°C for 15 min. The reaction mixture was subsequently cooled to 40°C over 2 min, diluted with 1 mL water, and purified via semi-preparative high performance liquid chromatography to yield pure [^{18}F]3-Fluoropropylazide (Column: Phenomenex Gemini 5 µm C18, 110 Å, 250x10mm; Mobile Phase A: Water, Mobile Phase B: Acetonitrile, Program: 10–35% in 30 min; Standard retention time: 21 min. The [^{18}F]3-Fluoropropylazide product was diluted in 20 mL H_2O and trapped on two Sep-Pak C18 plus short cartridge (waters) and eluted with 2 mL of DMSO.

In a separate vial, a solution of the following was prepared: 1. sterile water (50 µL), 2. copper(II) sulfate in water 10 µL of a 25 mg/mL solution), 3. benzimidazole ligand tripotassium 5,5',5"-[2,2',2"-nitrilotris(methylene)tris(1*H*-benzimidazole-2,1-diyl)]tripentanoate hydrate ($BimC_4A)_3$ (Sigma-Aldrich) (10 µL of a 0.025 mg/µL solution), and 4. ascorbic acid (20 µL of a 0.2 mg/µL solution). To this solution,

alkyne hydroxyl dendrimer precursor (3–5 mg, PANAM G4-OH alkyne$_{10}$) was added. Finally, the [^{18}F]3-Fluoropropylazide product in 2 mL DMSO was also added, and the whole vial was stirred at 40°C for 25 min. Then, it was diluted with 2 mL water and purified via semi-preparative HPLC (Phenomenex Biosec-SEC-s-2000, 300 x 1.2 mm; Mobile Phase: 9 g/L NaCl in water; Program: isocratic at 5 mL/min, Standard retention time: 11–14 min) to yield pure [^{18}F]OP-801. [^{18}F]OP-801 was trapped directly after HPLC on a C18 plus lite cartridge (Waters) and washed with 10 mL of water, then eluted with 1mL of ethanol and 9mL of saline. The Final product was checked for chemical and radiochemical purity via analytical HPLC (Phenomenex Jupiter 5µm C18, 300 Å, LC column, 250x4.6 mm; Mobile Phase A: Water with 0.1% TFA, Mobile Phase B: Acetonitrile with 0.1% TFA; gradient program: 5% B hold for1 min, 5–95% in 19 min at 1mL/min; [^{18}F]OP-801 retention time: 10 min; optimal wavelength 203nm).

Specific activity was determined by measuring the product area of the 203 nm peak on analytical HPLC and computing radioconcentration by comparing the area to a standard curve and measuring the amount of activity in a 100 µL sample.

Tracer evaluation study design: Stability of [^{18}F]OP-801 was assessed using *ex vivo* plasma samples from healthy female C57BL/6 mice (n = 4). Dynamic PET/CT imaging of female C57BL/6 mice injected with LPS (n = 6) or saline (n = 5) was performed to determine the optimal timepoint for obtaining high signal-to-background static scans. Static PET/CT images were acquired at the optimal timepoint of 50–60 min post-tracer injection for all LPS (n = 14) and saline (n = 6) mice. Uptake and biodistribution of [^{18}F]OP-801 was quantified in organs from a subset of mice (n = 7 LPS, n = 6 saline) using a gamma counter, and further evaluated in brain regions using high-resolution *ex vivo* autoradiography (n = 7 LPS, n = 6 saline). The numbers of mice analyzed for each experiment are listed in **Supplemental Table 1**.

Tracer stability: Formulated tracer (150–250 µCi, 25µCi/µg in saline and 10% ethanol) was injected into n = 4 female C57BL/6 mice by tail vein to evaluate *in vivo* stability of [^{18}F]OP-801 at 150 min post-injection using previously reported methods[22]. Briefly, 300–500 µL blood samples were collected via cardiac puncture and immediately centrifuged at 1800*g* for 4 min at room temperature to separate plasma. Each plasma sample was transferred to a tube containing acetonitrile and mixed thoroughly. Water was then added to each tube and centrifuged at 9400*g* for 4 min. The resulting supernatants were collected and analyzed via the same HPLC method used for quality control of [^{18}F]OP-801.

LPS PET/CT imaging: 24 hours after intraperitoneal administration of LPS (10 mg/kg in 100 µL saline, n = 14) or saline alone (n = 6), mice were anesthetized using isoflurane gas (2.0-3.5% for induction and 1.0-2.5% for maintenance) and formulated tracer (150–250 µCi in saline and 10% ethanol) was administered by tail vein. A 60-min dynamic PET scan was commenced just prior to tracer administration, and data was acquired in list mode format throughout the scan using the Inveon D-PET scanner (Siemens). The resulting data was binned and reconstructed into 19 time frames (4x15s, 4x60s, 11x300s). The PET system can deliver 1.5mm spatial resolution at the center of the 12.7mm field of view. Isotropic resolution was achieved using OSEM3D/MAP reconstruction algorithms with 18 subsets and 2 iterations and a

matrix size of 128x128x159. Static PET images (10 min) were acquired 50 min post-injection of [^{18}F]OP-801. The timepoint for static brain imaging of 50–60 min post-injection of [^{18}F]OP-801, was selected based on statistical testing of dynamic PET data and clearance considerations. After 50 min, tracer that has not been taken up will have already been mostly cleared to the kidney. CT scans were subsequently collected to provide attenuation correction and an anatomic reference for the PET data using the GNEXT scanner (Sofie), by transferring the mice in the same bed used in the Inveon PET scanner to ensure ease of co-registration. Brain PET images were quantified by first co-registering PET and CT images followed by fitting a standard brain atlas within the skull of each mouse (VivoQuant 4.0, inviCRO) using our previously described methods[23]. PET data is expressed as a percent injected dose per gram (%ID/g). Symptoms after LPS challenge were assessed using a standard murine sepsis score (MSS)[24] (scoring rubric in **Supplemental Table 2**) and three LPS-injected mice with negligible symptoms (score less than 3) were excluded from subsequent analysis. Mice were considered “low severity” with summed total scores between 3–6, and “high severity” with scores above 7. Four mice were imaged without scoring. After imaging, all mice underwent cardiac puncture followed by perfusion with saline (20 mL) to remove blood from organs to enable quantification of tracer uptake in tissues of interest.

Biodistribution and autoradiography: Organs were dissected, weighed, and placed into a gamma counter to measure radioactivity. Tracer distribution within the brain was further evaluated using high resolution autoradiography of 40 µm-thick sagittal brain slices. Brain slices used for autoradiography were subsequently stained with cresyl violet to enable assessment of [^{18}F]OP-801 uptake in specific brain regions; one saline and one LPS animal were excluded from all *ex vivo* analyses due to poor perfusion.

Statistics: GraphPad Prism (v9.01) was used to perform statistical analyses of brain atlas and gamma counting. All data was assessed for normalization, and parametric (multiple unpaired t-tests for *ex vivo* biodistribution and static PET brain atlas) and non-parametric (Mann-Whitney for all TACs and blood signal) tests were applied. A p-value ≤ 0.05 was considered significant.

Results

Radiochemistry: [^{18}F]OP-801 was reproducibly synthesized in excellent radiochemical purity (> 95%), specific activity (ranged from 52 to 12 µCi/µg over the course of the study), and yields conducive to preclinical in vivo imaging studies (4.3 ± 1.5% yield, n = 8 syntheses, decay-corrected to the starting fluoride ion) via a two-step synthetic process as detailed above: [^{18}F]3-fluoropropy azide (16.7 ± 4.6% decay-corrected intermediate yield) was synthesized using a Tracerlab FX-N radiosynthesis platform (GE Healthcare) prior to copper catalyzed click chemistry with alkyne hydroxyl dendrimer precursor, performed manually, to afford [^{18}F]OP-801. The order of mixing copper(II) sulfate, $(BimC_4A)_3$, and ascorbic acid was found to be particularly important – i.e., ascorbic acid must be added after copper(II) sulfate and $(BimC_4A)_3$. Total synthesis time for [^{18}F]OP-801 was approximately 2 hours.

Plasma stability: *In vivo* stability of [^{18}F]OP-801 was confirmed in healthy mice by *ex vivo* detection of 97 ± 3% intact radiotracer in the plasma of mice 150 min after injection. See **Supplemental Fig. 1** for HPLC chromatograms.

Dynamic PET/CT imaging and ex vivo biodistribution studies: Whole body PET/CT images revealed visually increased signal in tissues known to be inflamed following intraperitoneal LPS challenge, including brain, lung, and major abdominal organs such as the liver (Fig. 1, Supplemental Video 1). There is also elevated signal in the heart and carotid arteries of LPS-injected mice which reflects increased tracer in blood. PET images of saline-injected mice on the other hand show high levels of activity primarily restricted to the kidneys and bladder, due to renal clearance of [^{18}F]OP-801 known to occur when it is not actively taken up by target cells (Fig. 1).Time activity curves of liver and lung reveal significantly higher PET signal in LPS- versus saline-injected mice (liver: p = 0.01, lung: p = 0.003) (Fig. 2A). Likewise, quantitation of whole brain time activity curves demonstrated significantly elevated signal in LPS- versus saline-injected mice (p = 0.02) (Fig. 2B).*Ex vivo* biodistribution data confirmed PET findings for saline (n = 5) versus LPS (n = 6) mice, showing significant differences in tissues expected to have elevated infiltrating reactive innate immune cells, including brain (9.1±19.56 LPS vs. 0.3±0.43 saline %ID/g, p = 0.030), intestines (small: 20.4±15.56 LPS vs. 4.5±3.80 saline %ID/g, p = 0.017; large: 18.4±9.68 LPS vs. 4.8±4.07 saline %ID/g, p = 0.009), liver (27.0±30.11 LPS vs. 2.7±2.20 saline %ID/g, p = 0.009), lung (26.2±26.47 LPS vs. 2.9±4.34 saline %ID/g, p = 0.030), spleen (21.4±18.24 LPS vs. 2.0±1.60 saline %ID/g, p = 0.004), and stomach (13.2±7.09 LPS vs. 3.9±2.94 saline %ID/g, p = 0.017) (Fig. 3). Standard deviations are quite high in LPS mice due to the range in MSS score (0 to 15). Standard deviations are lower in saline mice, and within expected normal variability explained by occasional blood spots in lung and other tissues, although the brain was always clear after perfusion.

Static PET/CT brain imaging and ex vivo autoradiography: Brain PET/CT images (summed 50–60 min) revealed linearly increasing [^{18}F]OP-801 uptake, shown in Fig. 4A and **Supplemental Video 2**, correlating with severity of sepsis symptoms using the MSS (R = 0.854, p < 0.0001) for the mice that were scored (Fig. 4C). Brain atlas analysis of 50–60 min summed PET images showed an increase in signal throughout most brain regions, with significant differences (p < 0.05) between LPS- and saline-treated mice in the cortex, medulla, olfactory bulb, and pons (Fig. 4B). High resolution autoradiography overlaid on the same Nissl-stained brain slices revealed elevated tracer signal in similar regions identified through brain atlas analysis of PET images (Fig. 5), including the cortex, olfactory bulb, and brain stem, in addition to the cerebellum, hippocampus, white matter, and ventricles.

Discussion

In this study, we sought to synthesize, characterize, and demonstrate utility of a novel PET tracer specific for activated macrophages/microglia to enable detection of innate immune activation *in vivo.* We synthesized this novel hydroxyl dendrimer radiotracer,[^{18}F]OP-801, in high purity and suitable yields for *in vivo* testing and demonstrated its stability in healthy mice. Importantly, we found elevated [^{18}F]OP-801-

signal in regions/tissues known to be inflamed in mice following LPS challenge, in both peripheral and CNS tissues, and that the extent of tracer uptake in whole brain and liver correlated with sepsis score/severity.

[^{18}F]OP-801 was reproducibly synthesized in two steps. Synthesis of [^{18}F]3-fluoropropylazide was performed on an automated GE Tracerlab synthesis platform, however, low trapping efficiency and subsequently low [^{18}F]3-fluoropropylazide recovery (40–50%) was a key limiting factor in improving yield. That is, [^{18}F]fluoropropylazide was found to possess a relatively high affinity for both water and acetonitrile, necessitating reduction of both total volume and percentage of acetonitrile in the collected product fraction following semipreparative HPLC. Preliminary screening studies to optimize trapping and elution efficiency demonstrate that trapping and elution efficiency of [^{18}F]3-fluoropropylazide is inversely proportional to both total volume of water passed over the SepPak as well as percentage of acetonitrile by volume. To that end, optimization studies to modify HPLC conditions to minimize acetonitrile content in the mobile phase are underway. A second important consequence of relatively low initial yields for [^{18}F]OP-801 is subsequent low concentration of this key intermediate in the CuAAC reaction solution, requiring a relatively high starting mass of hydroxyl dendrimer alkyne precursor, which in turn potentially limits molar activity. Future studies will focus on optimizing the yield of [^{18}F]fluoropropyl-azide to enable reduction of starting mass of alkyne precursor without a significant drop in RCY or reproducibility. Finally, the second reaction (CuAAC to yield [^{18}F]OP-80-1) needed to be performed manually in a fume hood and involved addition of ^{18}F]fluoropropyl-azide to the prepared solution of alkyne precursor and click reagents. Efforts are currently underway to optimize and fully automate both steps so they can be performed on the same synthesis module in a streamlined and reproducible manner.

Prior to initiating *in vivo* studies in LPS-injected mice, we evaluated [^{18}F]OP-801 stability in healthy mice. As expected, we did not see metabolic breakdown of OP-801 in HPLC analysis of *ex vivo* plasma samples, consistent with previous work proving stability of hydroxyl dendrimers[25] and the fact that there are no cleavable bonds in the OP-801 structure. Importantly, the relative high signal observed in bone in biodistribution quantification is therefore not due to defluorination but is most likely attributed to tracer uptake bone marrow-resident myeloid cells.

Intraperitoneal injection of LPS in mice is a commonly used model to study systemic inflammation and microglial activation [26], and is thus well-suited for preliminary evaluation of our new tracer, [^{18}F]-OP-801, which is taken up by activated microglia and macrophages[27]. Specifically, we were interested in investigating the regional uptake of [^{18}F]-OP-801 and how the resulting PET signal relates to sepsis symptoms following LPS challenge. The MSS is a measure of sepsis symptoms including response to stimuli, appearance, respiration rate/quality, and level of activity/consciousness (as detailed in Supplemental Table 2). Crucially, we found a significant correlation between MSS and the *in vivo* uptake of [^{18}F]OP-801 in whole brain of LPS mice ($p < 0.0001$). Interestingly, for peripheral tissues, the liver was the only organ with a significant correlation between radioactive signal and MSS score ($p = 0.04$). Although the spleen is an important organ in the context of LPS challenge, we were unable to accurately

quantify the PET signal in this tissue due to significant signal spillover from the left kidney, which is adjacent to the spleen. Thus, immediately after PET imaging we removed the spleen from each mouse and quantified the radioactivity in this tissue using a gamma counter. When we compared the gamma counting signal in spleen to MSS there was no significant correlation. Taken together, our results indicate that the inflammation we detected in the brain and liver of LPS mice, using [^{18}F]OP-801 is highly associated with murine sepsis symptoms. This was not the case for other peripheral tissues collected during biodistribution studies.

LPS-induced behavior and symptoms vary with dose, application route, and time point following administration, among other factors[28]. Many studies have shown that after a single high dose of LPS, mice exhibit cognitive and behavioral changes along with heterogeneous microglia proliferation and activation throughout regions of the brain[28]. This heterogeneous activation of microglia throughout the entire brain has previously been described, in particular in the cortex, hippocampus, cerebellar white matter[29], and circumventricular organs (CVOs) lining the ventricles[30], and is consistent with the regions we identified as having high tracer signal in this study using both PET and *ex vivo* autoradiography. Whole brain time activity curves were divided by heart time activity curves as an estimation for radioactive signal in tissue versus blood over time. Of note, the level of brain/heart signal in LPS mice remained at a relatively high and steady level compared to the declining level observed in saline-treated mice throughout the scan. Numerically, the slope of brain/heart signal was found to be lower for LPS compared to saline-injected mice (-0.43 versus − 0.72, Supplemental Fig. 2). Taken together, these data indicate that the increased %ID/g in the brains of LPS mice could be due to slower washout from this tissue, potentially due to tracer uptake in activated microglia/macrophages.

In healthy mice, rapid clearance of [^{18}F]OP-801 was observed through the kidneys into the bladder which is consistent with what is known about the elimination route of hydroxyl dendrimers[31]. Importantly, there was no significant difference in radioactive signal in the kidneys between mice injected with LPS or vehicle, as quantified by *ex vivo* gamma counting. Since we were unable to reliably collect urine from all mice due to multiple mice voiding their bladders immediately prior to or after scanning, we cannot definitively conclude that the clearance rate for [^{18}F]OP-801 is the same between vehicle- and LPS-treated mice, however our kidney data indicates that this might be the case.

The mechanism of [^{18}F]OP-801 uptake is via fluid-phase endocytosis. [^{18}F]OP-801 has no receptor or ligand-binding component. In the presence of leaky vasculature, the tracer is better able to cross the blood-brain barrier and circulate throughout the brain. Unless myeloid cells are actively phagocytosing, the tracer will not be taken up. This specificity for reactive microglia/macrophages has been shown in previous publications, based on experimental evidence in > 40 models in six species [15,16,19,31]. In brief, [^{18}F]OP-801 diffuses rapidly in tissue and clears quickly from blood and other healthy tissues. Healthy, actively dividing cells are not quick enough to endocytose the dendrimer. At the site of pathology however, the dendrimer gets into the affected region(s) and is selectively taken up by the reactive microglia with

enhanced endocytosis rate. The ligand-free, biophysics-based uptake of the dendrimer is valuable from a practical standpoint where differential receptor expression in different conditions will not affect uptake.

One key limitation of our study was the high degree of variability in symptom severity between LPS-injected mice, which introduces a high variance into biodistribution and PET data; our plot correlating the MSS score with uptake does address this, but mice are not stratified in other analyses. Future work will include evaluating and characterizing tracer uptake and distribution in other models of neuroinflammation including experimental autoimmune encephalomyelitis (EAE). This will be an important step towards our intended use of this tracer in neurological diseases in humans.

Conclusion

[^{18}F]OP-801 has potential for highly sensitive and specific detection of activated macrophages/microglia in the whole body and brain. Based on our promising proof-of-concept data in LPS mice, we are motivated to evaluate the utility of [^{18}F]OP-801 for visualizing innate immune activation in additional mouse models of neuroinflammation and for measuring response to novel immunomodulatory treatments. We hope to use [^{18}F]OP-801 for patient stratification and monitoring responses to such therapies in the future.

Declarations

Acknowledgements: The authors would like to acknowledge Ashvattha Therapeutics, NSF GRFP Grant Number: DGE – 1656518 for funding.

Author Contributions: M.L.C. conceptualization, methodology, formal analysis, investigation, radiochemistry methodology and investigation, writing original draft, creating figures. E.C.A., S.R., I.A, S.N. investigation, manuscript review and editing. I.M.J. Radiochemistry conceptualization, methodology, and investigation, manuscript writing and editing. R.K. Radiochemistry methodology and investigation, manuscript review and editing. J.B.C., R.S. Radiochemistry conceptualization and methodology, manuscript review and editing. M.B., J.C. Supervision, funding acquisition, manuscript review and editing. B.S. Radiochemistry conceptualization, methodology, and investigation, supervision, manuscript writing and editing. M.L.J. Conceptualization, study design, data interpretation, manuscript writing and editing, supervision, funding acquisition.

Conflict of Interest Statement: M.L.C., I.M.J., C.A., B.S., and M.L.J receive research funding and materials from Ashvattha Therapeutics. M.B., R.S., and J.C. are employees of Ashvattha Therapeutics.

References

1. Werry EL, Bright FM, Piguet O, Ittner LM, Halliday GM, Hodges JR, Kiernan MC, Loy CT, Kril JJ, Kassiou M. Recent developments in TSPO PET imaging as a biomarker of neuroinflammation in

neurodegenerative disorders. International journal of molecular sciences. 2019;20(13):3161.

2. Krause DL, Müller N. Neuroinflammation, microglia and implications for anti-inflammatory treatment in Alzheimer's disease. International journal of Alzheimer's disease. 2010;2010.
3. Lambert J-C, Heath S, Even G, Campion D, Sleegers K, Hiltunen M, Combarros O, Zelenika D, Bullido MJ, Tavernier B. Genome-wide association study identifies variants at CLU and CR1 associated with Alzheimer's disease. Nature genetics. 2009;41(10):1094–1099.
4. Alam MM, Lee J, Lee SY. Recent Progress in the Development of TSPO PET Ligands for Neuroinflammation Imaging in Neurological Diseases. Nuclear Medicine and Molecular Imaging. 2017;51(4):283–296. doi:10.1007/s13139-017-0475-8
5. Chaney A, Becker E, Jackson IM, James ML. PET Imaging of Neuroinflammation. In: Ross, Gambhir, editors. Molecular Imaging. 2020.
6. Henningfield CM, Cleland JL, Sharma R, Green KN. Selective targeting of plaque-associated microglia through systemic dendrimer administration in an Alzheimer's disease model. Alzheimer's & Dementia. 2020;16(S2):e040661. https://doi.org/10.1002/alz.040661. doi:https://doi.org/10.1002/alz.040661
7. Jain P, Chaney AM, Carlson ML, Jackson IM, Rao A, James ML. Neuroinflammation PET imaging: current opinion and future directions. Journal of Nuclear Medicine. 2020;61(8):1107–1112.
8. Gui Y, Marks JD, Das S, Hyman BT, Serrano-Pozo A. Characterization of the 18 kDa translocator protein (TSPO) expression in post-mortem normal and Alzheimer's disease brains. Brain pathology. 2020;30(1):151–164.
9. Owen DR, Yeo AJ, Gunn RN, Song K, Wadsworth G, Lewis A, Rhodes C, Pulford DJ, Bennacef I, Parker CA, et al. An 18-kDa translocator protein (TSPO) polymorphism explains differences in binding affinity of the PET radioligand PBR28. Journal of cerebral blood flow and metabolism : official journal of the International Society of Cerebral Blood Flow and Metabolism. 2012;32(1):1–5. https://pubmed.ncbi.nlm.nih.gov/22008728. doi:10.1038/jcbfm.2011.147
10. Stanley ER, Chitu V. CSF-1 receptor signaling in myeloid cells. Cold Spring Harbor perspectives in biology. 2014;6(6):a021857. https://pubmed.ncbi.nlm.nih.gov/24890514. doi:10.1101/cshperspect.a021857
11. Spinelli F, Mu L, Ametamey SM. Radioligands for positron emission tomography imaging of cannabinoid type 2 receptor. Journal of Labelled Compounds and Radiopharmaceuticals. 2018;61(3):299–308.
12. Kannan S, Dai H, Navath RS, Balakrishnan B, Jyoti A, Janisse J, Romero R, Kannan RM. Dendrimer-based postnatal therapy for neuroinflammation and cerebral palsy in a rabbit model. Science translational medicine. 2012;4(130):130ra46-130ra46.
13. Mishra MK, Beaty CA, Lesniak WG, Kambhampati SP, Zhang F, Wilson MA, Blue ME, Troncoso JC, Kannan S, Johnston M V, et al. Dendrimer brain uptake and targeted therapy for brain injury in a large animal model of hypothermic circulatory arrest. ACS nano. 2014;8(3):2134–2147. https://pubmed.ncbi.nlm.nih.gov/24499315. doi:10.1021/nn404872e

14. Perumal OP, Inapagolla R, Kannan S, Kannan RM. The effect of surface functionality on cellular trafficking of dendrimers. Biomaterials. 2008;29(24–25):3469–3476.
15. Zhang F, Nance E, Alnasser Y, Kannan R, Kannan S. Microglial migration and interactions with dendrimer nanoparticles are altered in the presence of neuroinflammation. Journal of Neuroinflammation. 2016;13(1):1–11.
16. Nance E, Zhang F, Mishra MK, Zhang Z, Kambhampati SP, Kannan RM, Kannan S. Nanoscale effects in dendrimer-mediated targeting of neuroinflammation. Biomaterials. 2016;101:96–107.
17. Turk BR, Nemeth CL, Marx JS, Tiffany C, Jones R, Theisen B, Kambhampati S, Ramireddy R, Singh S, Rosen M. Dendrimer–N-acetyl-L-cysteine modulates monophagocytic response in adrenoleukodystrophy. Annals of neurology. 2018;84(3):452–462.
18. Niño DF, Zhou Q, Yamaguchi Y, Martin LY, Wang S, Fulton WB, Jia H, Lu P, Prindle Jr T, Zhang F. Cognitive impairments induced by necrotizing enterocolitis can be prevented by inhibiting microglial activation in mouse brain. Science translational medicine. 2018;10(471):eaan0237.
19. Alnasser Y, Kambhampati SP, Nance E, Rajbhandari L, Shrestha S, Venkatesan A, Kannan RM, Kannan S. Preferential and increased uptake of hydroxyl-terminated PAMAM dendrimers by activated microglia in rabbit brain mixed glial culture. Molecules. 2018;23(5):1025.
20. Cai KC, van Mil S, Murray E, Mallet J-F, Matar C, Ismail N. Age and sex differences in immune response following LPS treatment in mice. Brain, Behavior, and Immunity. 2016;58:327–337. https://www.sciencedirect.com/science/article/pii/S0889159116303592. doi:https://doi.org/10.1016/j.bbi.2016.08.002
21. Klein SL, Flanagan KL. Sex differences in immune responses. Nature Reviews Immunology. 2016;16(10):626–638. https://doi.org/10.1038/nri.2016.90. doi:10.1038/nri.2016.90
22. James ML, Shen B, Zavaleta CL, Nielsen CH, Mesangeau C, Vuppala PK, Chan C, Avery BA, Fishback JA, Matsumoto RR, et al. New Positron Emission Tomography (PET) Radioligand for Imaging σ-1 Receptors in Living Subjects. Journal of Medicinal Chemistry. 2012;55(19):8272–8282. https://doi.org/10.1021/jm300371c. doi:10.1021/jm300371c
23. Chaney AM, Johnson EM, Cropper HC, James ML. PET Imaging of Neuroinflammation Using [11C]DPA-713 in a Mouse Model of Ischemic Stroke. JoVE. 2018;(136):e57243. https://www.jove.com/t/57243. doi:doi:10.3791/57243
24. Shrum B, Anantha R V, Xu SX, Donnelly M, Haeryfar SMM, McCormick JK, Mele T. A robust scoring system to evaluate sepsis severity in an animal model. BMC Research Notes. 2014;7(1):233. https://doi.org/10.1186/1756-0500-7-233. doi:10.1186/1756-0500-7-233
25. Tunki L, Kulhari H, Bhargava SK, Pooja D. 4 - Pharmacokinetic considerations in design of dendrimer-based nanomedicines. In: Chauhan A, Kulhari HBT-PA of D, editors. Micro and Nano Technologies. Elsevier; 2020. p. 93–106. https://www.sciencedirect.com/science/article/pii/B9780128145272000044. doi:https://doi.org/10.1016/B978-0-12-814527-2.00004-4

26. Catorce MN, Gevorkian G. LPS-induced Murine Neuroinflammation Model: Main Features and Suitability for Pre-clinical Assessment of Nutraceuticals. Current neuropharmacology. 2016;14(2):155–164. https://pubmed.ncbi.nlm.nih.gov/26639457. doi:10.2174/1570159x14666151204122017
27. Zhao J, Bi W, Xiao S, Lan X, Cheng X, Zhang J, Lu D, Wei W, Wang Y, Li H, et al. Neuroinflammation induced by lipopolysaccharide causes cognitive impairment in mice. Scientific Reports. 2019;9(1):5790. https://doi.org/10.1038/s41598-019-42286-8. doi:10.1038/s41598-019-42286-8
28. Furube E, Kawai S, Inagaki H, Takagi S, Miyata S. Brain Region-dependent Heterogeneity and Dose-dependent Difference in Transient Microglia Population Increase during Lipopolysaccharide-induced Inflammation. Scientific Reports. 2018;8(1):2203. https://doi.org/10.1038/s41598-018-20643-3. doi:10.1038/s41598-018-20643-3
29. Hart AD, Wyttenbach A, Perry VH, Teeling JL. Age related changes in microglial phenotype vary between CNS regions: grey versus white matter differences. Brain, behavior, and immunity. 2012;26(5):754–765. https://pubmed.ncbi.nlm.nih.gov/22155499. doi:10.1016/j.bbi.2011.11.006
30. Silverman HA, Dancho M, Regnier-Golanov A, Nasim M, Ochani M, Olofsson PS, Ahmed M, Miller EJ, Chavan SS, Golanov E, et al. Brain region-specific alterations in the gene expression of cytokines, immune cell markers and cholinergic system components during peripheral endotoxin-induced inflammation. Molecular medicine (Cambridge, Mass.). 2015;20(1):601–611. https://pubmed.ncbi.nlm.nih.gov/25299421. doi:10.2119/molmed.2014.00147
31. Zhang F, Trent Magruder J, Lin Y-A, Crawford TC, Grimm JC, Sciortino CM, Wilson MA, Blue ME, Kannan S, Johnston M V, et al. Generation-6 hydroxyl PAMAM dendrimers improve CNS penetration from intravenous administration in a large animal brain injury model. Journal of controlled release : official journal of the Controlled Release Society. 2017;249:173–182. https://pubmed.ncbi.nlm.nih.gov/28137632. doi:10.1016/j.jconrel.2017.01.032

Scheme 1

Scheme 1 is not available with this version

Figures

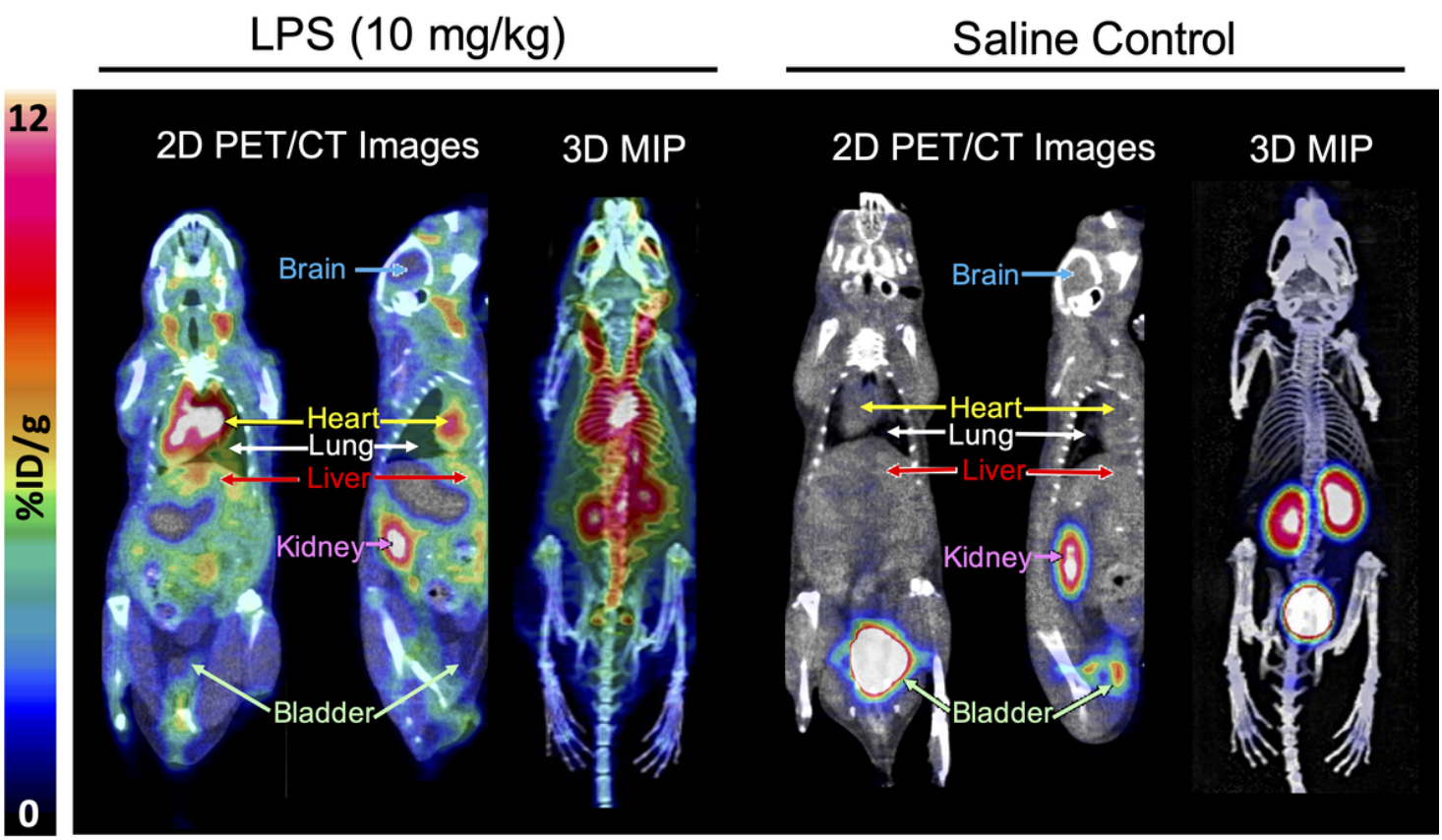

Figure 1

Whole body PET/CT images show visually higher uptake of [^{18}F]OP-801 in multiple tissues known to be inflamed in LPS-injected mice, including brain, liver, and lung. Conversely, signal in saline-injected mice is restricted to bladder and kidney, reflecting radiotracer excretion. Arrows highlight signal in organs of interest in 2D PET images.

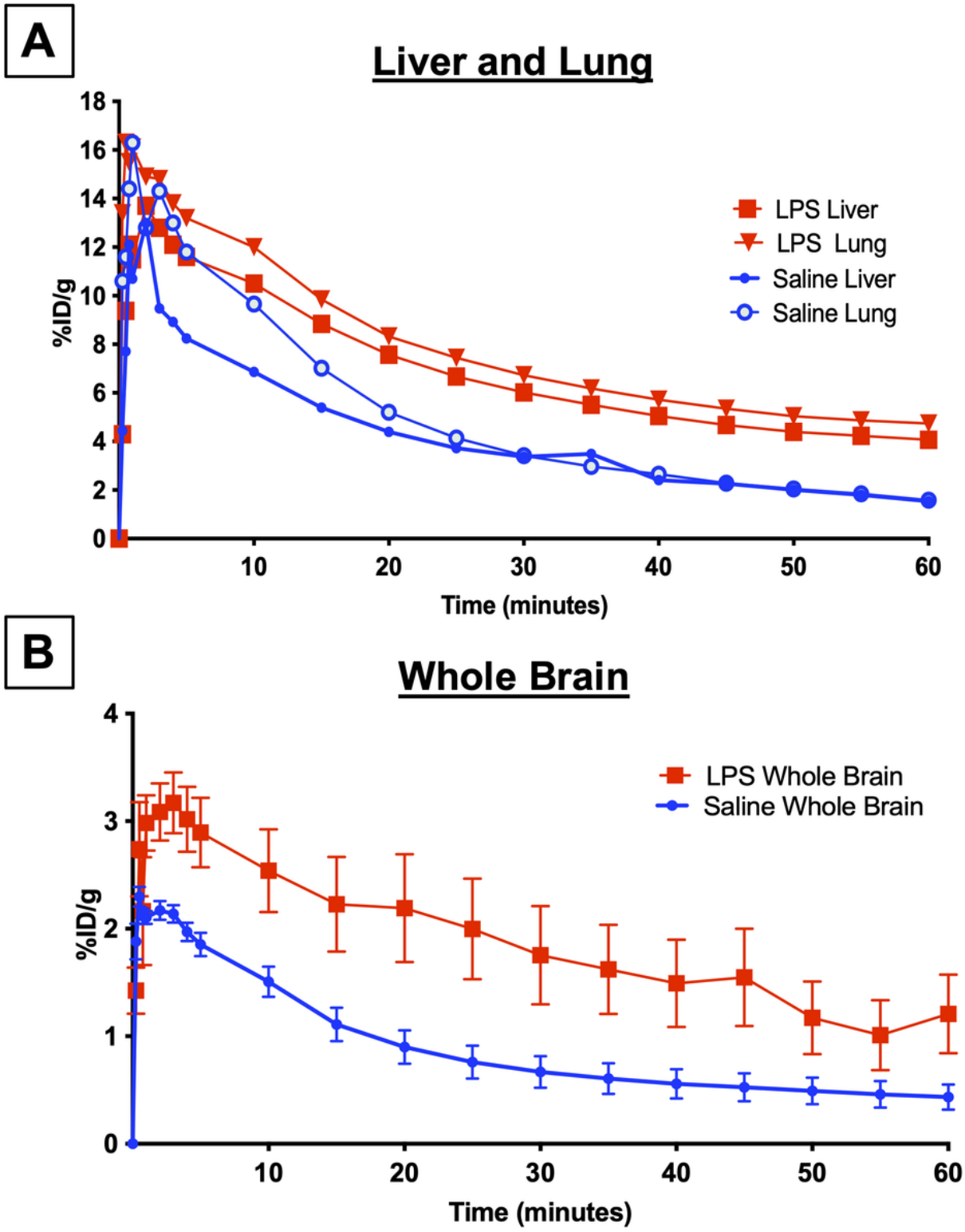

Figure 2

Time activity curves of [^{18}F]OP-801 uptake in **A.** liver and lung, and **B.** whole brain of mice treated with saline (n=5) or LPS (n=6), liver P=0.01, lung P=0.003, brain P=0.02.

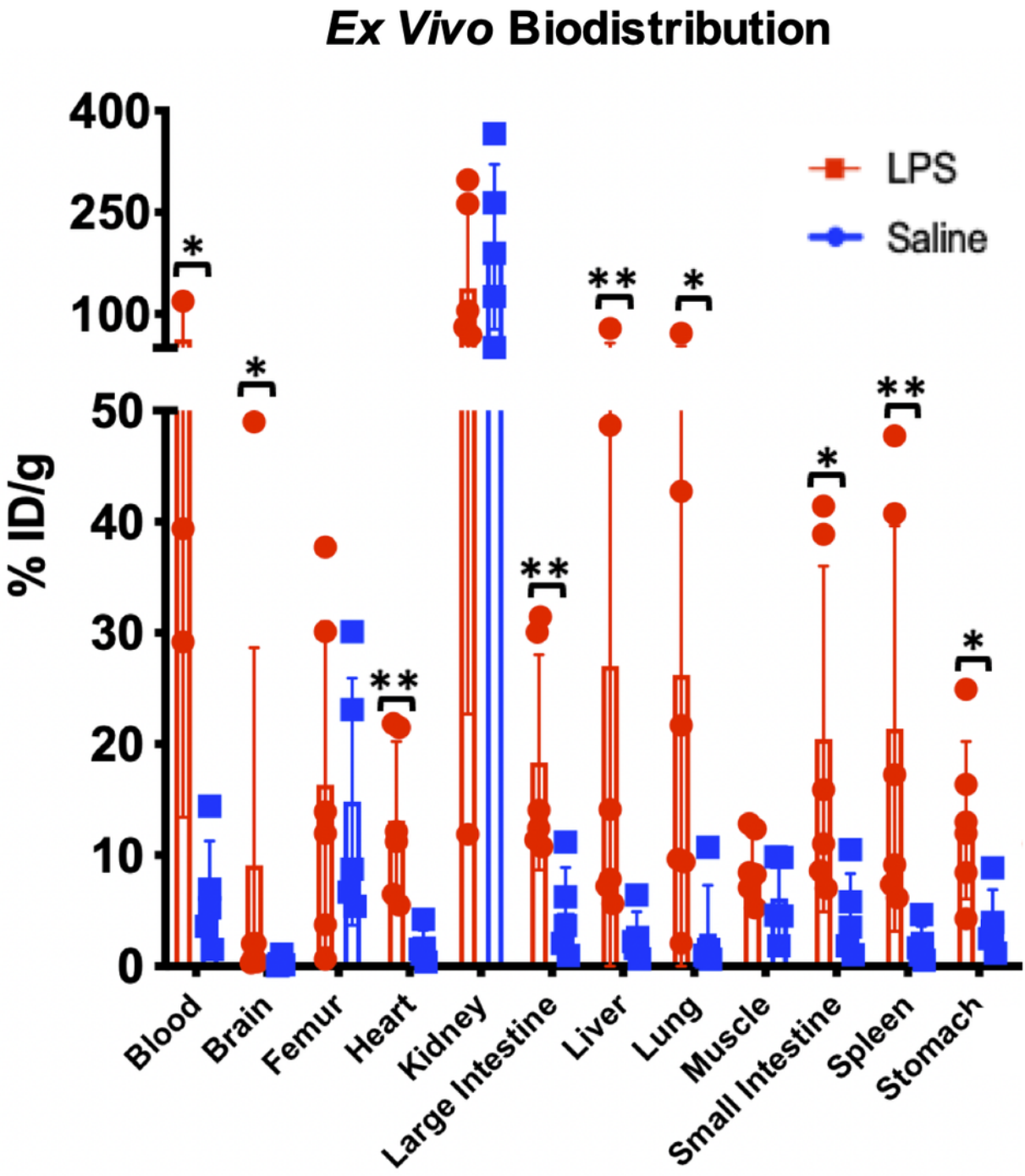

Figure 3

Ex vivo gamma counting of blood and perfused organs from mice treated with saline (n=5) or LPS (n=6), 70 min after injection of [^{18}F]OP-801. *: $p<0.05$ **: $p<0.01$

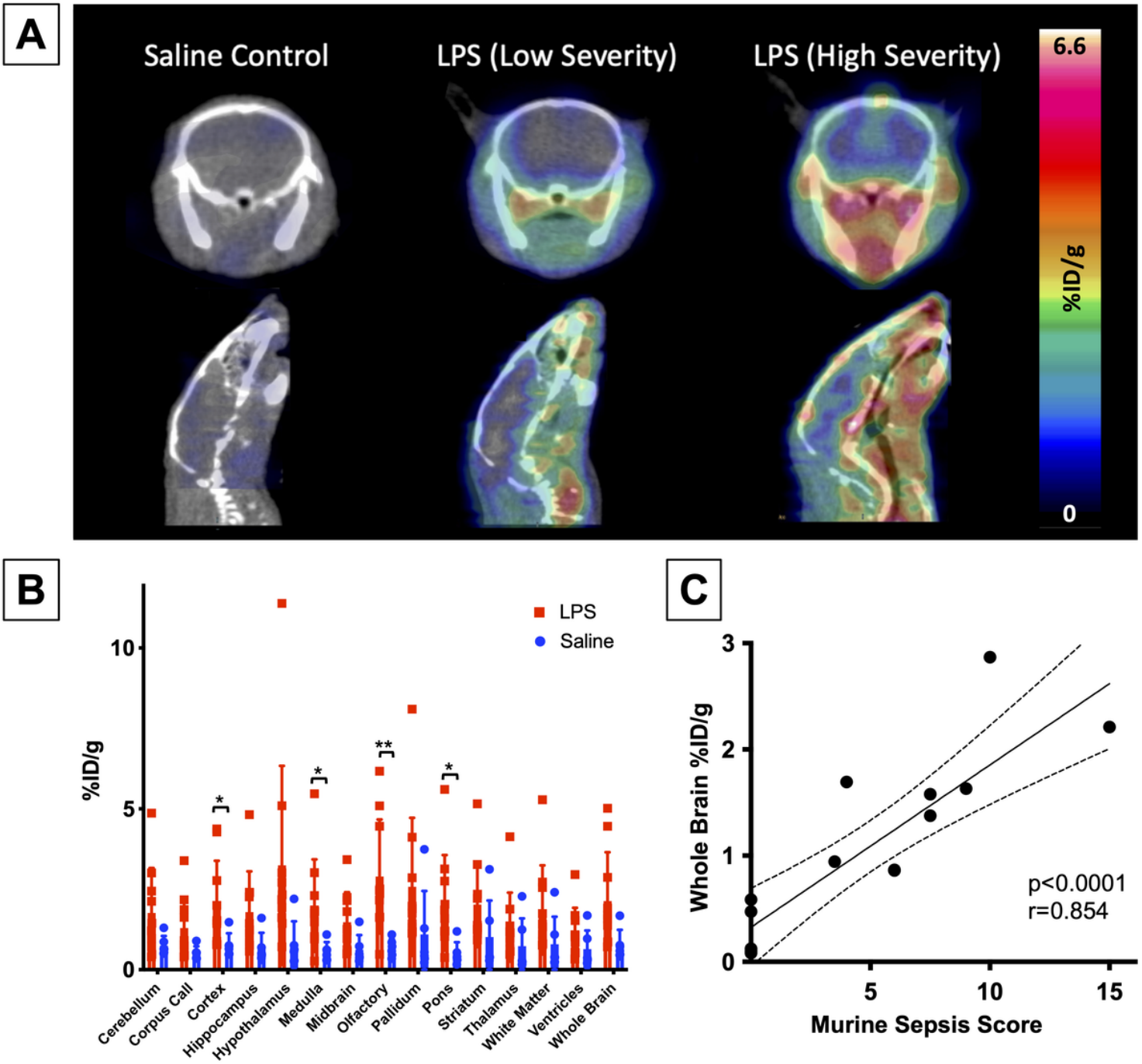

Figure 4

A. Representative summed mouse brain PET/CT images 50-60 min after tracer administration and 24 hours after injection of saline or LPS (10 mg/kg). Mice injected with LPS displayed varying murine sepsis scores indicative of their symptom severity – here we show PET images of mice with low and high sepsis scores and demonstrate the ability of [^{18}F]OP-801 to detect increasing levels of inflammation in a manner that correlates with symptom severity. **B.** Quantification of tracer uptake in brain regions from mice treated with saline (n=6) or LPS (n=11) using summed 50-60 min PET images. *: p<0.05 **: p<0.01. **C.** Plot of LPS MSS scores versus %ID/g in whole brain from 50-60 min PET, with linear regression and 95% confidence intervals shown.

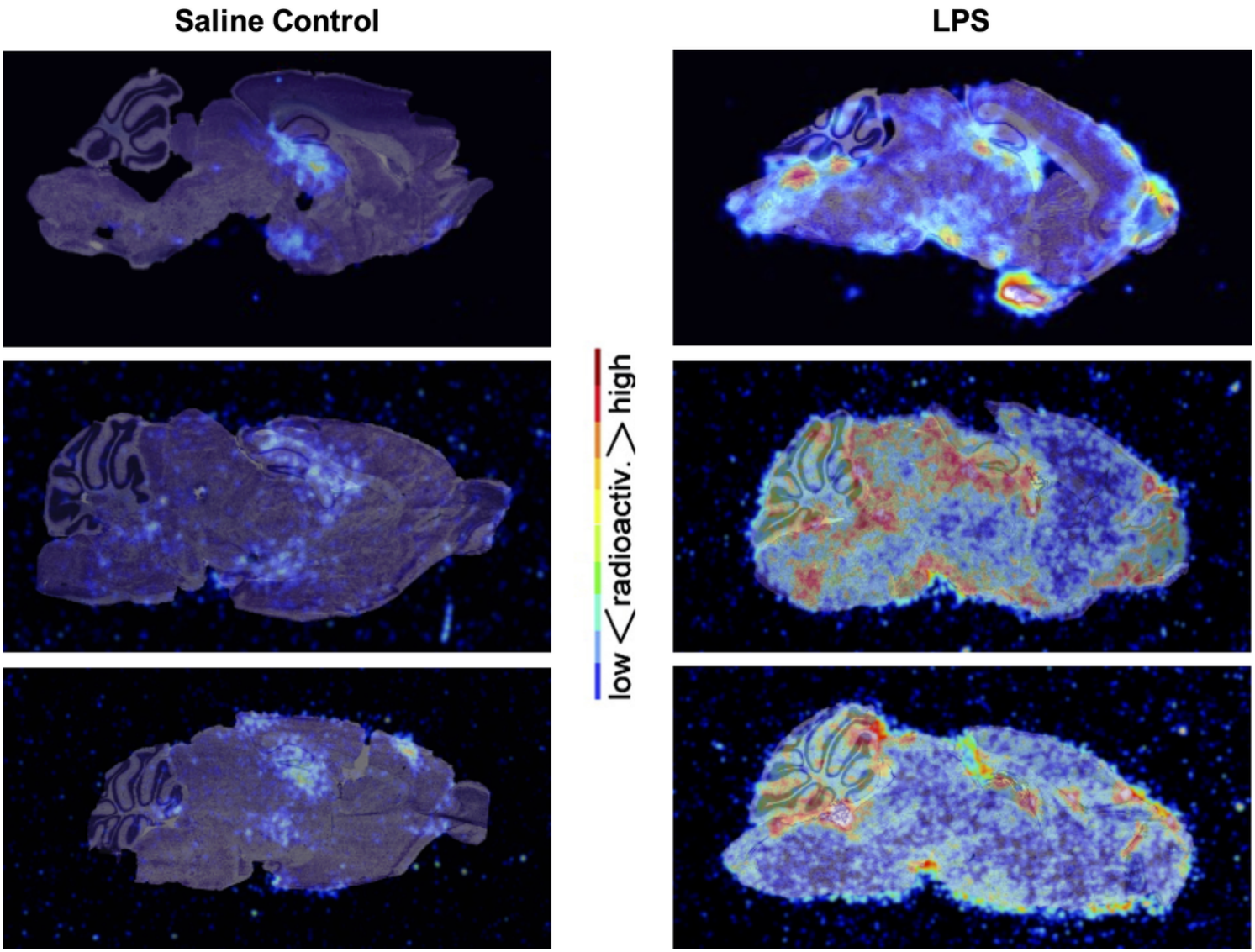

Figure 5

Ex vivo autoradiography of 40 µm-thick sagittal brain slices from representative saline versus high-MSS LPS mouse, 70 min after [^{18}F]OP-801 injection and 25 hours after LPS administration, 20-hour exposure, overlaid on Cresyl violet (Nissl) stain of same slice.

Supplementary Files

This is a list of supplementary files associated with this preprint. Click to download.

- SupplementalLPSOP801paper24July2023.docx